

# Diffraction tomography for biological cells imaging using digital holographic microscopy

I. Bergoënd, C. Arfire, N. Pavillon, C. Depeursinge

Ecole Polytechnique Fédérale de Lausanne (EPFL), Applied Photonics Laboratory, 1015 Lausanne (Switzerland)

## ABSTRACT

Many biological objects are mainly transparent and weakly scattering, thus a promising (and already widely used) way of imaging them consists in considering optical refractive index variations. The method proposed here permits 3D imaging of the refractive index distribution with a tomographic approach. Usually, the classical Radon transform does not sufficiently take into account the physical interaction between light and biological cells, therefore diffraction has to be considered.

Diffraction tomography is a method that permits 3D reconstruction of the refractive index, using many captures of the complex optical field, for example at various angles. Then, the 3D Fourier space can be filled with spatial frequencies coming from the different views. Our setup consists in rotating the object under fix illumination and detection. The complex scattered field needed for tomographic reconstruction is obtained from digital holographic microscopy, using one hologram per angle of view. The method is first validated with a spherical object. Mie scattering theory is used to simulate the measured field from which the tomographic reconstruction is performed. Experimental results on microbeads are also presented. The wide capability of 3D imaging using diffraction tomography in biology is shown.

**Keywords:** Diffraction tomography, digital holography, microscopy, 3D.

## 1. INTRODUCTION

Optical tomography is a very promising 3D imaging technique, especially due to its non-invasive property. It has been studied for several years but the progress from two towards three dimensions is quite recent due to increasing computing capabilities. One main method to perform tomography involves spatial gating, as in OCT and related techniques.

From the previously published works, tomographic reconstructions with multiple angles of view have been obtained using, on the one hand, Radon transform and, on the other hand, diffraction tomography. In optical imaging, Radon transform can be applied on intensity or phase images. It is usually applied in X-rays imaging but has been found to be valid for weak-scattering objects having slow variations compared to the wavelength<sup>1</sup>. Diffraction tomography is a more physical approach. It has to be applied on entire complex fields and is also valid for quite weak scatterers when the first Born or Rytov approximation is used.

It has also been studied in the domains of ultrasounds<sup>2</sup>, acoustics applied to geophysics<sup>3</sup> and microwaves<sup>4</sup>. In optics, a special form has been developed to allow reconstructions on the basis of intensity images only<sup>5</sup>. Tomographic methods have also been developed using, for example, angular scanning of the incident beam<sup>6</sup>, multiple wavelength<sup>7</sup> or short coherence of the light (optical coherence tomography). The main works carried out concerning 2D imaging were reconstructions of the simulated Shepp and Logan's phantom<sup>8</sup> and simulated or measured cylinders like optical fibers<sup>9</sup>. Among the few published works about 3D reconstructions, one can find Radon reconstructions<sup>10</sup>, studies on the spatial frequencies covered by diffraction tomography<sup>11</sup> and refractive index reconstructions of biological objects in which calibration<sup>12</sup> or compensation for missing frequencies<sup>13</sup> are needed.

In this paper, digital holographic microscopy is explained in section 2. The capability of optical tomography to perform 3D imaging for biology is then presented through results obtained with Radon transform on biological specimens. The principle of diffraction tomography is described in section 4 and performances of the method are discussed. Preliminary results obtained in simulation and with experimental data are finally presented.

\*isabelle.bergoend@epfl.ch; phone 0041 (0)21 693 51 57; <http://apl.epfl.ch/muvision>

## 2. ACQUISITION AND PROCESSING: DIGITAL HOLOGRAPHIC MICROSCOPY

Digital holographic microscopy is an interferometric technique in which the interference pattern between a reference beam and the beam scattered by the object is recorded on a digital camera after passing through a microscope objective for image magnification. Here, only semi-transparent objects are investigated, and the setup is in transmission. For the purpose of tomography, the specimen under study is embedded into a rotating system. A sketch of such an experimental setup is presented on Figure 1.

The numerical reconstruction consists in retrieving the object field which can be considered as modulated by the interference pattern. This is done by selection of the proper region in the Fourier plane. After numerical propagation and compensation for the phase tilt and curvature and the optical aberrations, the complex field scattered by the object is obtained in the focus plane or at an arbitrary distance<sup>14</sup>. For the Radon transform, in which diffraction is neglected, we use focused images; however for diffraction tomography the complex scattered field at a known distance is needed. In that case, our digital holographic method has the advantage of requiring only one hologram acquisition per angle of view to compute the complex field.

Using this technique of digital holographic microscopy, the complex scattered field can be obtained with only one acquisition per orientation of the object, without any marker or destructive process.

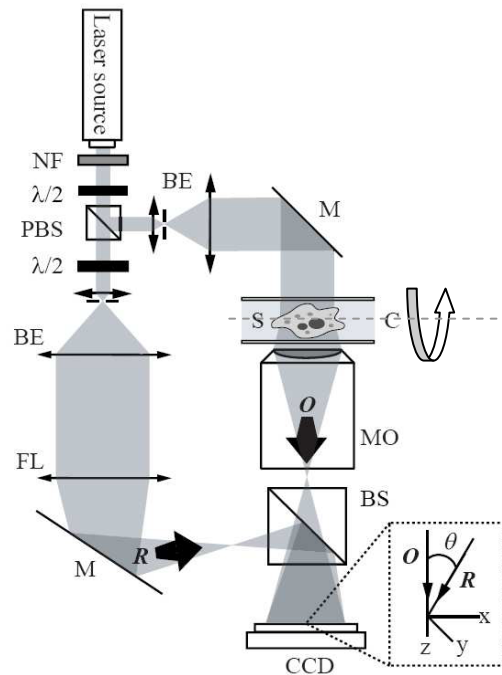


Figure 1. Principle of experimental setup for digital holographic microscopy in transmission. NF neutral filter;  $\lambda/2$  halfwave plate; MO microscope objective; FL field lens; M mirror; PBS polarizing beam splitter; BS beam splitter; O object wave; R reference wave; C specimen chamber; S specimen. Inset: detail showing the off-axis geometry at the incidence on the CCD.

## 3. OPTICAL TOMOGRAPHY IN BIOLOGY

### 3.1 Basic ideas of the Radon transform

The tomographic principle first described by Radon and implemented using a backprojection algorithm assumes straight line propagation inside and outside the object. This hypothesis is easily verified with X-rays inside a human body for example, but it may also be acceptable in optics with weak scatterers and slowly variations of the refractive index compared to the wavelength. For such objects, the measured phase map is related to the integrated optical path through

the object, therefore Radon's approach is valid. As our objects of interest are microscopic transparent specimens, phase is the relevant data. Because it will not be interpreted by the algorithm as physical phase information but as integrated optical paths, unwrapping is necessary. Focused phase maps are obtained for different positions of the object during one-axis rotation and the backprojection algorithm is applied.

### 3.2 Results from experimental data

On Figure 2, a 3D reconstruction of refractive index distribution obtained by this method is presented. The specimen is a tek amoeba (*Hyalosphenia papilio*). The rotation is achieved by clamping the observed specimen with a micropipette fixed on a motorized stage, so that it could be rotated within a chamber containing the immersion medium (glycerol,  $n=1.473$ ). The total angle of rotation is  $180^\circ$  with steps of  $1^\circ$ , the axis being perpendicular to the illumination direction. The sample is illuminated with a laser diode (wavelength: 635 nm), and imaged with a 0.4 NA 20X microscope objective. Figure 1 presents a visualization of the 3D reconstructed amoeba, whose shell is approximately 130  $\mu\text{m}$  long, 70  $\mu\text{m}$  wide and 35  $\mu\text{m}$  deep, where the internal structure can be readily identified. Some internal elements in the amoeba are a few microns in size, showing that the tomographic reconstruction is close to the optical resolution of the setup. The resolution in refractive index is approximately 0.01.

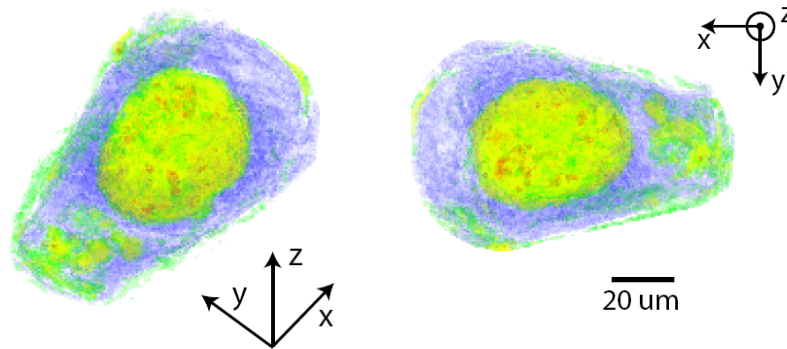


Figure 2. Transparency view of a tomographic measurement of a tek amoeba, in (a) angular view and (b) x-y projection. Colors correspond to refractive index value range: Blue: 1.448-1.467, Green: 1.474-1.478, Yellow: 1.478-1.493, Red: 1.493-1.513. White: refractive index of the immersion medium.

This example demonstrates the importance of developing optical tomography, especially for biological imaging without contact. By taking into account the physical phenomenon of diffraction of light in the object, a better resolution is expected for 3D reconstructions. The principle of diffraction tomography is presented in the next section.

## 4. PRINCIPLES OF DIFFRACTION TOMOGRAPHY

For optical tomography, Radon's approach does not take into account the physical nature of the interaction between light and matter, which is often not a simple phase delay encountered by straight rays. Therefore, an approach for diffraction tomography was developed by M. Born and E. Wolf in 1969 under the assumption of a weak scattering<sup>15</sup>. Especially, they show that their model can be seen as the consequence of considering a single scattering of photons inside the object. The scattering potential  $F$  of the object is defined as:

$$F(\vec{r}) = \frac{k^2}{4\pi} (n^2(\vec{r}) - 1) \quad (1)$$

where  $k = 2\pi/\lambda$  is the wavenumber for a wavelength  $\lambda$  and  $n(\vec{r})$  is the object spatial distribution of the refractive index to be reconstructed. The total scalar field  $U(\vec{r})$  can be written as the sum of the incident field  $U_i(\vec{r})$  and the

scattered field  $U_s(\vec{r})$ . Under the hypothesis of slowly varying  $n$  compared to  $\lambda$  and plane incident wave, the scattered field satisfies the equation:

$$\nabla^2 U_s(\vec{r}) + k^2 U_s(\vec{r}) = -4\pi F(\vec{r})U(\vec{r}) \quad (2)$$

By writing equation 2 in the form of an integral and choosing  $G(\vec{r} - \vec{r}')$  the 3D Green function of the Helmholtz operator to be  $G(\vec{r} - \vec{r}') = \frac{e^{ik|\vec{r} - \vec{r}'|}}{|\vec{r} - \vec{r}'|}$ , the following equation can be deduced:

$$U(\vec{r}) = U_i(\vec{r}) + \int_V F(\vec{r}')U(\vec{r}') \frac{e^{ik|\vec{r} - \vec{r}'|}}{|\vec{r} - \vec{r}'|} d^3r' \quad (3)$$

where  $V$  is a volume including the scattering object.

Assuming that the refractive index of the scattering object varies slowly and that it slightly departs from the index of the surrounding medium, the first-order Born approximation is obtained by replacing the total field  $U(\vec{r})$  with the incident field  $U_i(\vec{r})$  in equation 3 and thus get a linear equation:

$$U(\vec{r}) \approx U_i(\vec{r}) + \int_V F(\vec{r}')U_i(\vec{r}') \frac{e^{ik|\vec{r} - \vec{r}'|}}{|\vec{r} - \vec{r}'|} d^3r' \quad (4)$$

As  $U_i(\vec{r})$  is known to be a plane wave, this expression can be computed. By using the angular spectrum representation of the field, Born and Wolf finally show that, at a finite distance  $z$  from the object, some components of the 3D Fourier transform of  $F$  can be simply obtained from the 2D Fourier transform of the scattered field by the expression:

$$\tilde{F}(K_x, K_y, K_z) = \frac{f_z}{2\pi i} \tilde{U}_s(f_x, f_y; z; \vec{s}_0) e^{-if_z z} \quad (5)$$

In equation 5,  $\sim$  refers to the Fourier transform,  $\vec{s}_0$  is the direction of the incident beam,  $f_x$ ,  $f_y$  and  $f_z$  are spatial frequencies of the Fourier transform of  $U_s(\vec{r})$  and  $K_j = f_j - k\vec{s}_{0j}$  with  $j = x, y, z$ . This equation means that 3D spatial frequency components of the object can be computed from 2D Fourier transforms of the scattered field.

The computation of the reachable object frequencies  $K_j$  shows that each measurement of the scattered field in a given direction corresponds to a cap of sphere of same orientation in the Fourier space. Consequently, the frequency space is filled after a certain number of measurements with caps of spheres that ideally cover the entire spectrum.

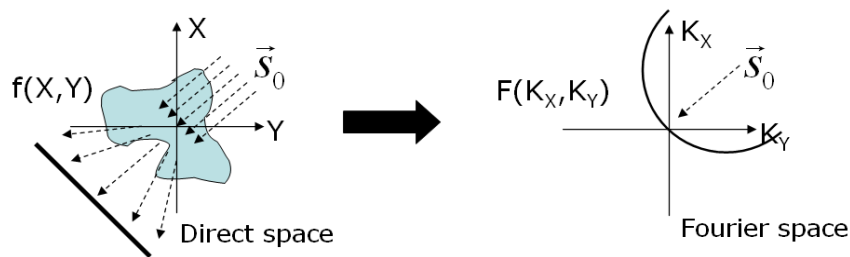


Figure 3. Measurement of the scattered field in the direction  $\vec{s}_0$  and its corresponding cap of sphere in the frequency space.

Under Born approximation, the theoretically reachable spatial frequencies are characterized by:

$$\sqrt{K_x^2 + K_y^2 + K_z^2} \leq \frac{4\pi}{\lambda} \quad (6)$$

However, the resolution of the microscope objective has to be taken into account because of the limitation it may induce in the Fourier space.

## 5. FIRST RESULTS IN DIFFRACTION TOMOGRAPHY

### 5.1 Results using data obtained in numerical simulation

Figure 5 presents the 3D reconstruction of a microbead obtained with simulated input data. The optical scattered field is computed from Mie theory<sup>16</sup> for a non-absorbing microbead of radius 4 microns and refractive index 1.55. The amplitude of the scattered field used for the reconstruction of Figure 5 is shown on Figure 4. The spatial scale is approximately the same for Figure 4 and Figure 5 a). The tomographic process was performed using 1000 angles of rotation randomly chosen in the 3D space. Due to the isotropy of the object studied here, the same scattered field is used for all angles. The surrounding medium has a refractive index of 1.54.

The bead size and the ratio between object and medium refractive indices are both well reconstructed. Figure 5 c) presents the imaginary part of the reconstructed refracted index. As expected, it is much lower than the real part (about 200 times): the non-absorbing property of the object has also been correctly retrieved.

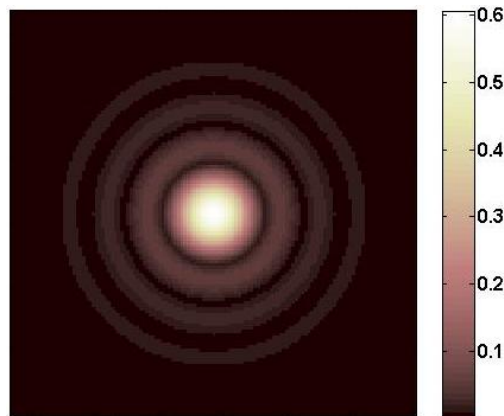


Figure 4. Amplitude of the scattered field computed from Mie theory for a microbead of radius 4 microns and refractive index 1.55 in a medium of index 1.54.

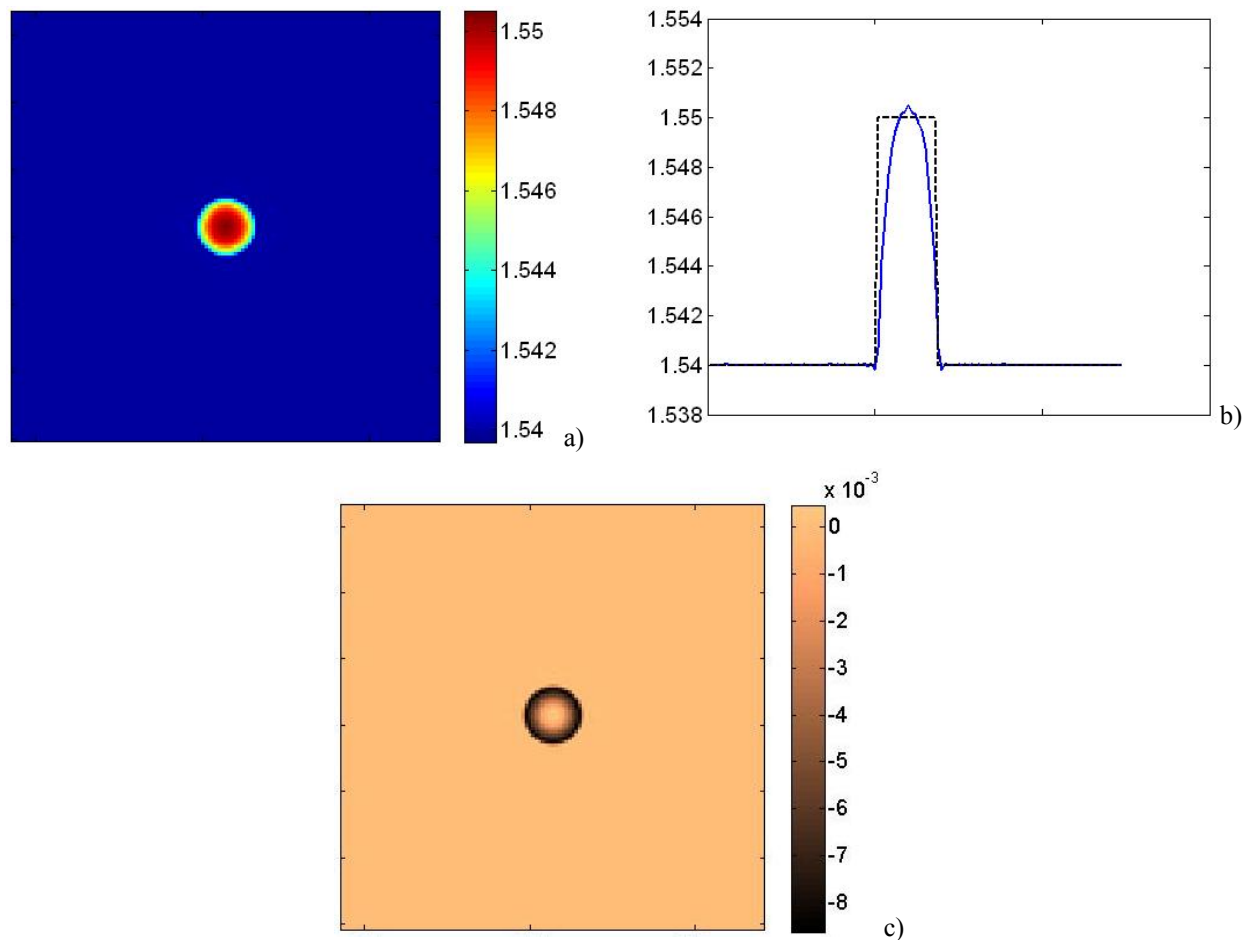


Figure 5. 3D reconstruction of a microbead from simulated input data. The amplitude of the input field is shown on Figure 4. a: Center section of the real part of the 3D refractive index reconstruction. b: Center profile of the 3D refractive index reconstruction. The dashed line stands for the expected index profile. c: Center section of the imaginary part of the refractive index, negligible compared to the real part a).

## 5.2 Results using measured data

Our first results concerning measured data have been obtained using a 63X magnification objective of NA 0.95. The object is a microbead of index 1.59 in a medium of index 1.56. Taking advantage of the isotropy of the object, one input image has been used for each direction in the reconstruction process. The total field has been obtained with the DHM technique. The incident field has been considered to be equal to the field measured in a region far from the bead.

As shown on , the reconstruction is satisfying. Some artifacts are visible, especially some circles (actually 3D spheres) in the bead section. They may be due to some local noise in the reconstruction that is made circular because of the use of a single input image.

More complex objects will now be imaged. It opens the way to promising applications of diffraction tomography with DHM.

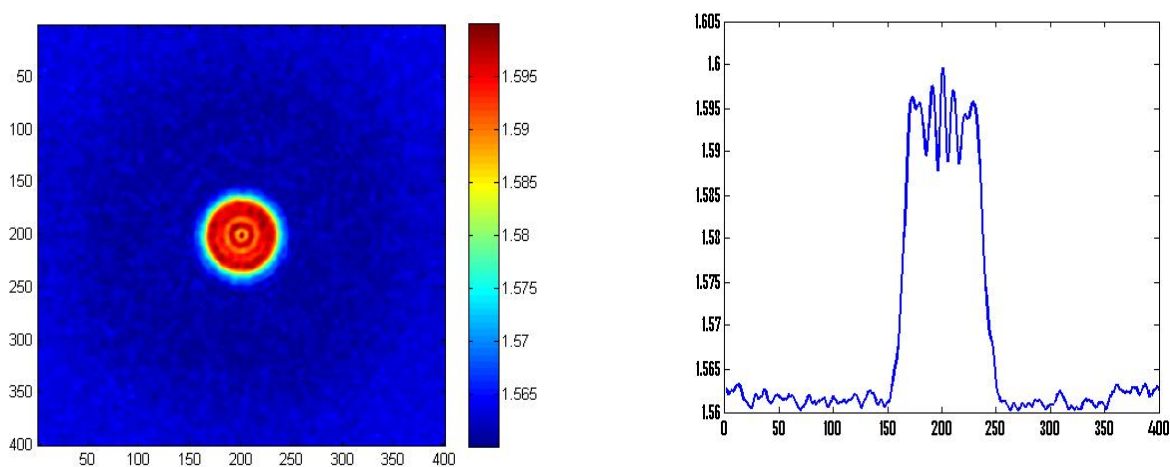


Figure 6: Reconstruction of an experimentally measured bead, section and profile, versus refractive index.

## 6. CONCLUSIONS

We have shown the importance of performing optical tomography for biological applications, and the advantage provided by the technique of digital holographic microscopy to obtain the complex scattered field in a short acquisition time. Preliminary results have been presented from simulated and experimental data, demonstrating the ability of tomography used together with digital holographic microscopy to reconstruct simple objects. They initiate a promising technique for 3D imaging of the inner parts of cells and small biological objects.

## 7. ACKNOWLEDGEMENTS

The research leading to these results has received funding from the European Community's Seventh Framework Programme FP7/2007-2013 under grant agreement n° 216105.

The authors wish to thank Olivier Seydoux from EPFL/LOA for his help on simulations of the scattered fields according to Mie theory.

## REFERENCES

1. Wedberg, T., Stamnes, J., and Singer, W., "Comparison of the filtered backpropagation and the filtered backprojection algorithms for quantitative tomography," *Applied Optics* 34, 6575–6581 (1995).
2. Sponheim, N., Gelius, L., Johansen, I., and Stamnes, J., "Quantitative results in ultrasonic tomography of large objects using line sources and curved detector arrays," *IEEE transactions on ultrasonics, ferroelectrics, and frequency control* 38, 370–379 (1991).
3. Gu, B. and Ji, Y., "Geophysical diffraction tomography," *Acoustical imaging* 18, 289–298 (1990).
4. Slaney, M., Kak, A., and Larsen, L., "Limitations of imaging with first-order diffraction tomography," *IEEE transactions on microwave theory and techniques* 32, 860–874 (1984).
5. Maleki, M., Devaney, A., and Schatzberg, A., "Tomographic reconstruction from optical scattered intensities," *J. Opt. Soc. Am. A* 9, 1356–1363 (1992).

6. Choi, W., Fang-Yen, C., Badizadegan, K., Oh, S., Lue, N., Dasari, R., and Feld, M., "Tomographic phase microscopy," *Nature Methods* 4, 717–719 (2007).
7. Montfort, F., Colomb, T., Charrière, F., Kuehn, J., Marquet, P., Cucho, E., Herminjard, S., and Depeursinge, C., "Submicrometer optical tomography by multiple-wavelength digital holographic microscopy," *Applied Optics* 45, 8209–8217 (2006).
8. Pan, S. and Kak, A., "A computational study of reconstruction algorithms for diffraction tomography: interpolation versus filtered backpropagation," *IEEE transactions on acoustics, speech and signal processing* 31, 1262–1275 (1983).
9. Chen, B. and Stamnes, J., "Validity of diffraction tomography based on the first born and the first Rytov approximations," *Applied Optics* 37, 2996–3006 (1998).
10. Charrière, F., Colomb, T., Cucho, E., Marquet, P., and Depeursinge, C., "Digital holographic microscopy applied to diffraction tomography of a cell refractive index," *Biomedical Optics*, TuH6 (2006).
11. Vertu, S., Delaunay, J., Yamada, I., and Haeberlé, O., "Diffraction microtomography with sample rotation: influence of a missing angle core in the recorded frequency space," *Cent. Eur. J. Phys.* 7, 22–31 (2009).
12. Debailleul, M., Georges, V., Simon, B., Morin, R., and Haeberlé, O., "High-resolution three-dimensional tomographic diffractive microscopy of transparent inorganic and biological samples," *Optics Letters* 34, 79–81 (2009).
13. Sung, Y., Choi, W., Fang-Yen, C., Badizadegan, K., Dasari, R., and Feld, M., "Optical diffraction tomography for high resolution live cell imaging," *Optics Express* 17, 266–277 (2009).
14. Colomb, T., Montfort, F., Kuehn, J., Aspert, N., Cucho, E., Marian, A., Charrière, F., Bourquin, S., Marquet, P., and Depeursinge, C., "Numerical parametric lens for shifting, magnification, and complete aberration compensation in digital holographic microscopy," *J. Opt. Soc. Am. A* 23, 3177–3190 (2006).
15. Born, M. and Wolf, E., [Principles of Optics, seventh (expanded) edition], Cambridge University Press (1999).
16. Bohren C.F. and Huffman D. R., [Absorption and scattering of light by small particles], Wiley-Interscience publication, New York, 82-116 (1983).